NAVAL POSTGRADUATE SCHOOL

MONTEREY, CALIFORNIA

THESIS

O(10-300M) SCALE VORTICITY AND DIVERGENCE IN THE NEARSHORE

by

Paul W. Lenz

June 2018

Thesis Advisor: James H. MacMahan
Second Reader: Mara S. Orescanin

Approved for public release. Distribution is unlimited.

THIS PAGE INTENTIONALLY LEFT BLANK

REPORT DOCUMENTATION PAGE			*Form Approved OMB No. 0704-0188*

1. AGENCY USE ONLY *(Leave blank)*	**2. REPORT DATE** June 2018	**3. REPORT TYPE AND DATES COVERED** Master's thesis

4. TITLE AND SUBTITLE O(10-300M) SCALE VORTICITY AND DIVERGENCE IN THE NEARSHORE	**5. FUNDING NUMBERS** RQLYT
6. AUTHOR(S) Paul W. Lenz	
7. PERFORMING ORGANIZATION NAME(S) AND ADDRESS(ES) Naval Postgraduate School Monterey, CA 93943-5000	**8. PERFORMING ORGANIZATION REPORT NUMBER**
9. SPONSORING / MONITORING AGENCY NAME(S) AND ADDRESS(ES) N/A	**10. SPONSORING / MONITORING AGENCY REPORT NUMBER**

11. SUPPLEMENTARY NOTES The views expressed in this thesis are those of the author and do not reflect the official policy or position of the Department of Defense or the U.S. Government.

12a. DISTRIBUTION / AVAILABILITY STATEMENT Approved for public release. Distribution is unlimited.	**12b. DISTRIBUTION CODE** A

13. ABSTRACT (maximum 200 words)

Submesoscale turbulence in the nearshore is observed with purpose-built drifters to perform Lagrangian measurements of the vorticity and divergence of flows with length scales under 300 meters and on-time scales of a few minutes to a few hours. Drifters are designed with an inexpensive GPS datalogger with position error of a few centimeters and velocity error of a few centimeters per second. An accelerometer is added for measuring the rotation rate of the drifters. The drifters are fitted with four vanes for a total diameter of 1 meter to capture the vorticity at 1-meter length scale. Vorticity and divergence of nearshore submesoscale flows exceed 10,000 times the Coriolis frequency (f), which is a large departure from the large-scale geostrophic flows in the ocean. The results of this experiment describe the nearshore surface vorticity and divergence, providing further insight into surface mixing at scales smaller than 300 meters.

14. SUBJECT TERMS nearshore, vorticity, divergence, drifter, DKP, dynamic kinematic properties	**15. NUMBER OF PAGES** 39
	16. PRICE CODE

17. SECURITY CLASSIFICATION OF REPORT	**18. SECURITY CLASSIFICATION OF THIS PAGE**	**19. SECURITY CLASSIFICATION OF ABSTRACT**	**20. LIMITATION OF ABSTRACT**
Unclassified	Unclassified	Unclassified	UU

NSN 7540-01-280-5500 Standard Form 298 (Rev. 2-89) Prescribed by ANSI Std. 239-18

THIS PAGE INTENTIONALLY LEFT BLANK

Approved for public release. Distribution is unlimited.

O(10-300M) SCALE VORTICITY AND DIVERGENCE IN THE NEARSHORE

Paul W. Lenz
Lieutenant Commander, United States Navy
BSME, University of Illinois at Urbana-Champaign, 2007

Submitted in partial fulfillment of the
requirements for the degree of

MASTER OF SCIENCE IN METEOROLOGY AND PHYSICAL OCEANOGRAPHY

from the

NAVAL POSTGRADUATE SCHOOL
June 2018

Approved by: James H. MacMahan
Advisor

Mara S. Orescanin
Second Reader

Peter C. Chu
Chair, Department of Oceanography

THIS PAGE INTENTIONALLY LEFT BLANK

ABSTRACT

Submesoscale turbulence in the nearshore is observed with purpose-built drifters to perform Lagrangian measurements of the vorticity and divergence of flows with length scales under 300 meters and on-time scales of a few minutes to a few hours. Drifters are designed with an inexpensive GPS datalogger with position error of a few centimeters and velocity error of a few centimeters per second. An accelerometer is added for measuring the rotation rate of the drifters. The drifters are fitted with four vanes for a total diameter of 1 meter to capture the vorticity at 1-meter length scale. Vorticity and divergence of nearshore submesoscale flows exceed 10,000 times the Coriolis frequency (f), which is a large departure from the large-scale geostrophic flows in the ocean. The results of this experiment describe the nearshore surface vorticity and divergence, providing further insight into surface mixing at scales smaller than 300 meters.

THIS PAGE INTENTIONALLY LEFT BLANK

TABLE OF CONTENTS

THIS PAGE INTENTIONALLY LEFT BLANK

LIST OF FIGURES

LIST OF TABLES

THIS PAGE INTENTIONALLY LEFT BLANK

ACKNOWLEDGMENTS

The field work was supported by the Office of Naval Research and technology development by the Gulf of Mexico Research Initiative. Appreciation is extended to the NPS field team (Tucker Freismith, Casey Gon, Paul Jessen, Keith Wyckoff) for their help with drifter design, construction and deployment. Special thanks to my advisor, Jamie MacMahan, for his support and assistance through the entire process.

THIS PAGE INTENTIONALLY LEFT BLANK

I. INTRODUCTION

Submesoscale turbulence in the ocean occurs at scales of a few meters to a few kilometers and contributes to the overall surface layer mixing (Capet et al. 2008; McWilliams 2016). Unlike large scale flows, submesoscale turbulence has a larger Rossby number that is on the order of 1, Ro = ζ/f, where ζ is the relative vertical vorticity and f is the local planetary vorticity (Ohlmann et al. 2016). At Ro >1, geostrophic balance breaks down and lateral shear becomes as important as planetary vorticity allowing for a forward energy cascade to dissipate energy from the larger scale flows (McWilliams et al. 2001; Muller et al. 2005; Molemaker et al. 2010).

Measuring submesoscale turbulence has proven to be challenging at smaller scales owing to the small size and short-time scale associated with these flows. Larger-scale flows from 10 to 100 km have been successfully measured using satellite altimetry (Lehahn et al. 2007; d'Ovidio et al. 2009) and shipboard hydrographic data (Rudnick 1996; Shearman et al. 1999; Mahadevan and Tandon 2006). At these larger scales, Rossby numbers are small and the flows are geostrophic. These flows also evolve on larger spatial and longer time scales that are within the margins of error associated with the instruments used to observe these large-scale flows.

Drifters have successfully and repeatedly been used to capture large-scale circulations in the ocean providing Lagrangian observations of the features that they are tracing (e.g., Swenson and Niiler 1996; LaCasce and Ohlmann 2003; Ohlmann et al. 2016). Clusters of drifters can be used to calculate the differential properties (DKP) of these features such as the vorticity, divergence, and shear. Previously, position error of small, inexpensive GPS-enabled loggers and the high cost and size of precision GPS-enabled loggers has allowed for only large-scale flows to be measured. Recent improvements in GPS technology have allowed for drifters to be used to calculate the DKP of ocean features down to 250 meters (Ohlmann et al. 2016).

This work builds on the efforts by Ohlmann et al. (2016) who found vorticity and divergence values upwards of 10f and 5f respectively for ocean scales ranging from 250 to

4000 meters (Ohlmann et al. 2016). Furthermore, they found a large increase in flow field variance at smaller length scales resulting from an accumulation of variance from each previous length scale. This work uses a similar approach to observe the DKP of features smaller than 250 meters in the nearshore with custom-built drifters with inexpensive GPS-enabled loggers. Post processing of the recorded GPS data allows for the observation of features smaller than 250 meters with position error of only a few centimeters and velocity errors of only a few centimeters per second. This study provides additional insight into how large vorticity and divergence can reach at smaller length scales (10-300 m) in the ocean as shown by the trend of increasing variance at smaller length scales previously observed.

II. METHODS AND FIELD EXPERIMENT

A. DRIFTER DESIGN

To capture vorticity down to 1 meter, nine vorticity drifters (Figure 1) were constructed with four equally spaced vertical drag fins attached to an 11-cm-diameter acrylic cylinder. Each drifter was 35 cm tall with matching height fins giving it a diameter of 1 m. Below the cylinder a weight was attached to stabilize the drifter by lowering its center of gravity. A 60-cm-diameter PVC disc was attached to the bottom to enhance stability and as a dampener to reduce the vertical motions and surfing effects (Schmidt et al. 2003). On the top of each drag fin, foam was added to provide enough buoyancy so only the 20-cm tall mast protruding from the removeable cap of the drifter was above the water line. Inside the waterproof acrylic cylinder housed the removeable battery, a Yost Labs 3-Space Datalogger Inertial Measurement Unit (IMU), and an Emlid Reach RS GPS datalogger (Emlid). The GPS antenna wire was routed through the mast, sealed, and attached to an external antenna.

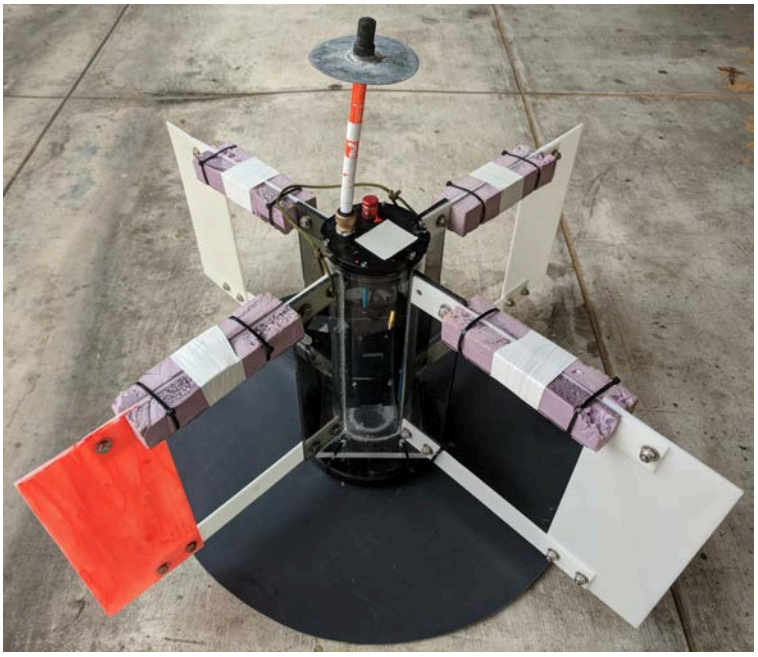

Figure 1. Picture of vorticity drifter with removeable cap designed to move along with ocean features while recording position and rotation rate.

Large survey-grade, less than 0.01-m position error, antennas were too heavy and bulky to be used on the vorticity drifter, so a small GPS patch antenna was sourced. These smaller antennas suffer from higher position error due to weak signal reception compared to multipathing noise (Saeki and Hori 2006). To minimize this noise, aluminum discs were installed under the patch antenna (MacMahan et al. 2009). To increase position accuracy further, survey-grade post processing software was used with base-station corrections from the National Geodetic Surveys Continuously Operating Reference Stations (CORS) network (https://www.ngs.noaa.gov/CORS/) on all GPS data observations from the drifters after all deployments.

Two different antennas were tested with the Emlid GPS datalogger to determine which provided the least relative position error. The Maruwa MWSL1203C GPS antenna and the Ethertronics GPS1002857 Quadhelix GPS antenna were each attached to individual Emlid Reach RS GPS dataloggers and each antenna was tested with and without the multipath reducing aluminum disc below it for a total of four test units. The four test units were placed on the roof with an unobstructed view of the sky in a line with approximately 15 cm of space between each one. Each Emlid GPS recorded the position of the stationary test units at 1 Hz for one hour. The observations for each antenna test unit were passed through survey-grade post processing software with CORS base-station corrections to improve position accuracy. The demeaned Easting (x) and Northing (y) position estimates were plotted (Figure 2) and the average relative position error (ε_h) was calculated using

$$\varepsilon_h = \sqrt{\frac{1}{N}\sum_{1}^{N}\left(x(t)^2 + y(t)^2\right)} \tag{1}$$

for each test unit where t was time. The Maruwa antenna had the smallest relative position error on the order of 8 cm.

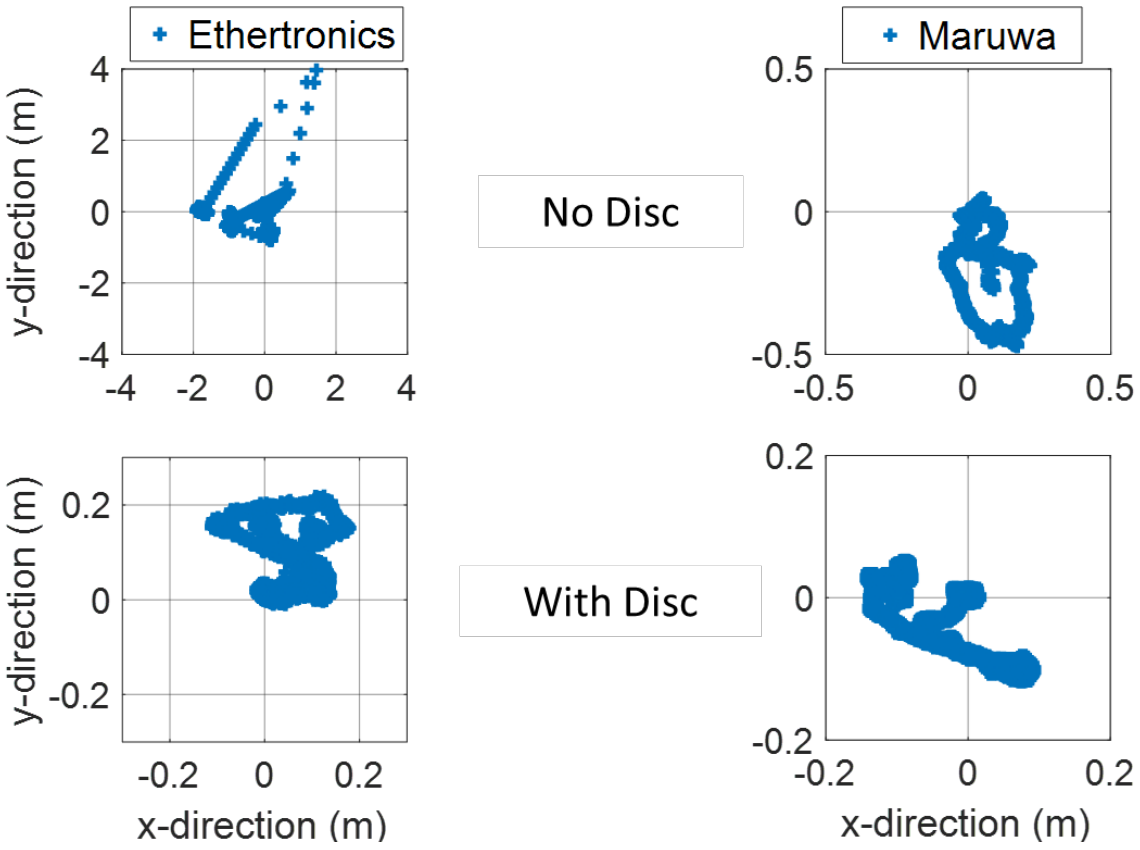

Figure 2. Demeaned position estimates for Ethertronics antenna (left) and Maruwa antenna (right) with disc to reduce multipathing (bottom) and without disc (top). Note the difference in scale for each antenna, left and right, and for the addition of the disc, top and bottom.

Even though all antennas remained stationary during the test, the relative position errors created velocities in the *x* and *y* directions that were calculated using forward-differencing and plotted (Figure 3) for each direction (*u*) and (*v*) respectively. From these estimated velocities, the average relative velocity error (ε_U) was calculated using

$$\varepsilon_U = \sqrt{\frac{1}{N}\sum_{1}^{N}\left(u(t)^2 + v(t)^2\right)} \tag{2}$$

for each test unit. The Maruwa antenna had the smallest relative velocity error on the order of 3 mm/s. Based on the results from the stationary test, the Maruwa antenna was selected to be used on all vorticity drifters.

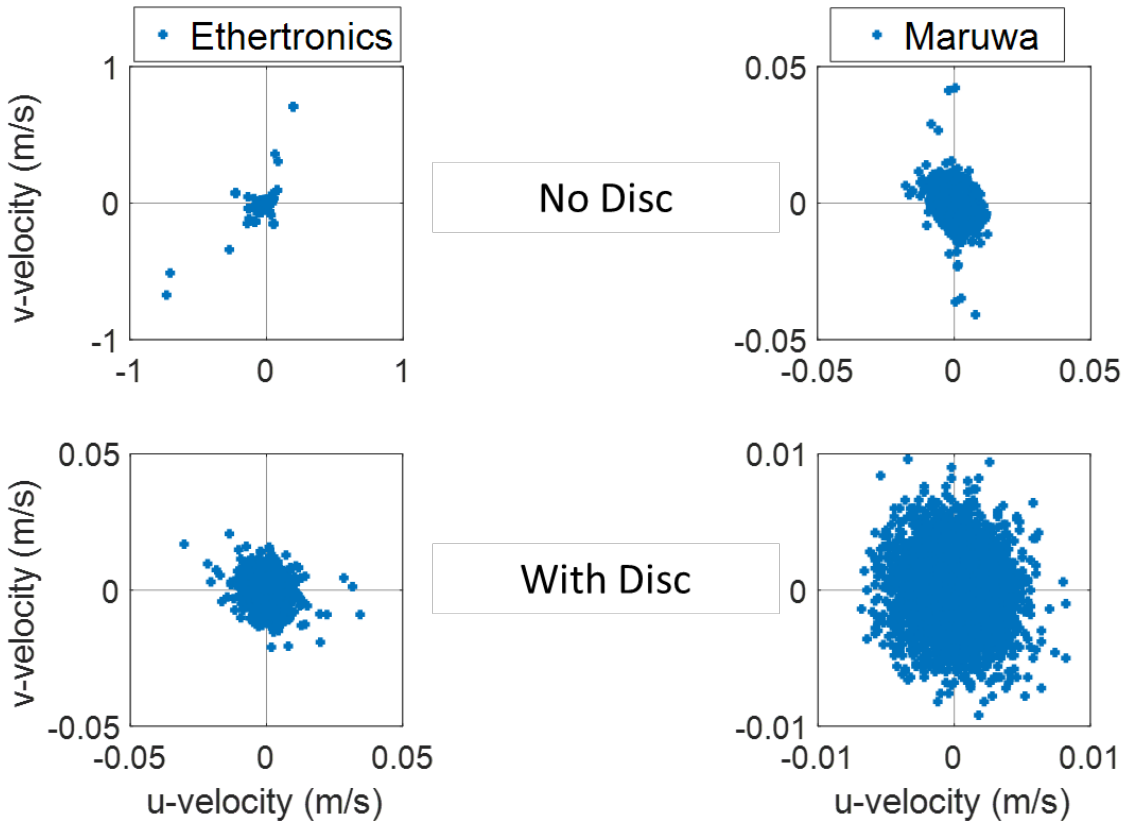

Figure 3. Corresponding velocities due to change in position estimate for Ethertronics antenna (left) and Maruwa antenna (right) with disc to reduce multipathing (bottom) and without disc (top). Note the difference in scale for each antenna, left and right, and for the addition of the disc, top and bottom.

The Emlid GPS dataloggers have two modes for ambiguity resolution, fix-and-hold and continuous. They also have the ability to set the elevation mask angle to exclude satellite signals below the mask angle selected to limit noisy measurements. To determine the best combination of these settings and modes for a moving drifter, a dynamic evaluation test was performed. Three combinations of elevation mask angle and ambiguity resolution mode were selected, 15-degree mask with fix-and-hold mode, 15-degree mask with continuous mode, and 25-degree mask with continuous mode. Similar to the testing procedure used by MacMahan et al. (2009), each combination was compared to a survey-grade (<1-cm horizontal error) Ashtech GPS base receiver and antenna by mounting the Ashtech GPS and the three Emlid GPS dataloggers onto a golf cart. The golf cart was pushed around a local track at speeds approximating those of an ocean drifter (Figure 4).

Since it was not possible to measure the exact offset between the Ashtech and Emlid antenna receiver recording positions, the antenna offsets were estimated using

$$Offset = \sqrt{\frac{1}{N}\sum_{1}^{N}\left[\left(x(t)_{Emlid} - x(t)_{Ashtech}\right)^2 + \left(y(t)_{Emlid} - y(t)_{Ashtech}\right)^2\right]} \quad (3)$$

for the post processed GPS points and with the offsets, the average position error (ε_h) for each Emlid GPS as compared to the Ashtech GPS was calculated using

$$\varepsilon_h = \sqrt{\frac{1}{N}\sum_{1}^{N}\left(\sqrt{\left[\left(x(t)_{Emlid} - x(t)_{Ashtech}\right)^2 + \left(y(t)_{Emlid} - y(t)_{Ashtech}\right)^2\right]} - Offset\right)^2} \quad (4)$$

on the order of 11 cm for the Emlid GPS datalogger with the 15-degree elevation masking angle setting and fix-and-hold mode selected. The speed of the Emlid GPS and the Ashtech GPS were significantly correlated at 95% with $R^2 = 0.99$ (Figure 3). The average moving speed error (ε_U) between the Emlid GPS speed (U_{Emlid}) and the Ashtech ($U_{Ashtech}$) was calculated using

$$\varepsilon_U = \sqrt{\frac{1}{N}\sum_{1}^{N}\left(U(t)_{Emlid} - U(t)_{Ashtech}\right)^2} \quad (5)$$

and found to be on the order of 0.7 cm/s for the Emlid GPS datalogger with 15-degree elevation masking angle setting and fix-and-hold mode selected. Moving speed errors were found to be independent of speed as well (Figure 4). Based on the results from the dynamic evaluation test, the fix-and-hold ambiguity resolution mode with a 15-degree elevation masking angle were set on all Emlid GPS dataloggers used in the vorticity drifters.

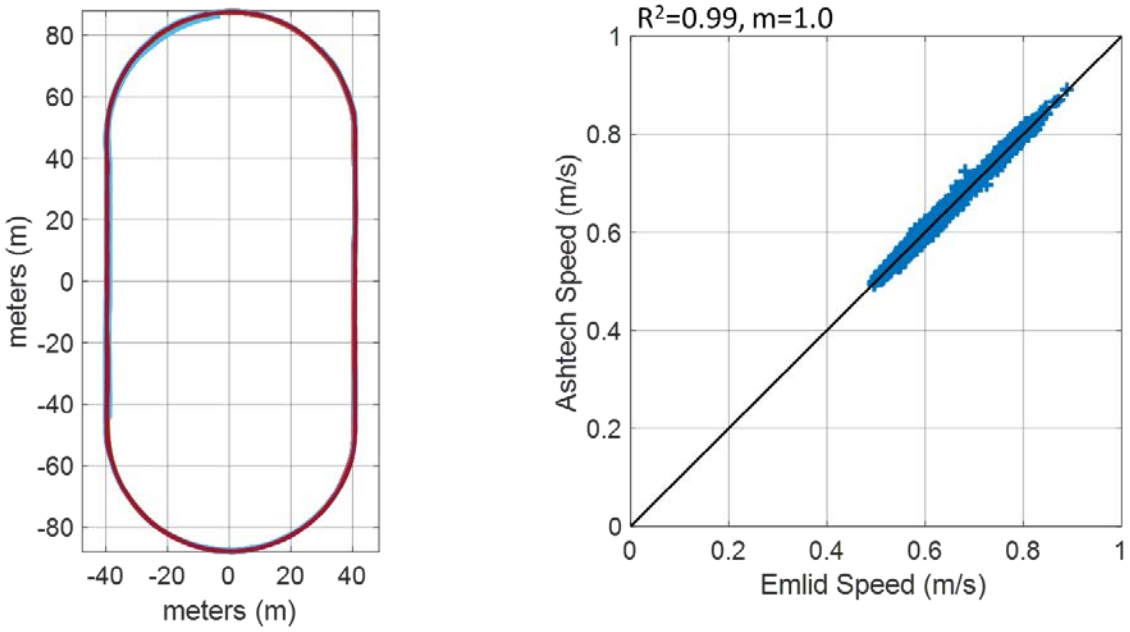

Figure 4. Demeaned position estimates for Ashtech and Emlid GPS dataloggers showing shape of local track walked (left). Comparison of Ashtech and Emlid GPS estimated speeds with 15-degree elevation masking angle setting and fix-and-hold mode selected.

B. DEPLOYMENTS

The experiment consisted of multiple deployments of up to nine vorticity drifters deployed in a 3 x 3 square pattern with approximatley 50 meters of spacing between each drifter in areas that were visually energetic (Table 1). The locations chosen were in highly energetic areas along fronts and eddies off Point Sal, California, from 12–14 September 2017 and again off of several points on the southern coast of Monterey Bay on 11 October 2017 and 14 March 2018. Deployment times were between 11 and 160 minutes each. Each drifter recorded its position via the GPS and rotation rate via the IMU at 1 Hz and stored the data on internal memory.

Table 1. Summary of vorticity drifter deployments.

Overall deployment #	Date	Location	Deployment of that Day	Deployment Time Length (minutes)
1	12 SEP 2017	Point Sal	A	104
2	12 SEP 2017	Point Sal	B	160
3	13 SEP 2017	Point Sal	A	80
4	13 SEP 2017	Point Sal	B	118
5	13 SEP 2017	Point Sal	C	101
6	14 SEP 2017	Point Sal	A	52
7	14 SEP 2017	Point Sal	B	11
8	14 SEP 2017	Point Sal	C	14
9	14 SEP 2017	Point Sal	D	30
10	14 SEP 2017	Point Sal	E	35
11	14 SEP 2017	Point Sal	F	27
12	11 OCT 2017	Monterey	A	37
13	14 MAR 2018	Monterey	A	69

C. DIFFERENTIAL PROPERTIES (DKP) CALCULATIONS

All GPS observations were post processed using the survey-grade post processing software and 30-second block averages of the observation points were taken to minimize the effects of wave motion on the drifter observations. A forward differencing scheme was used to determine the velocities (u and v) of each block averaged observation. Converting individual drifter observations into two-dimensional DKP values required a drifter cluster for computation. Using four drifters in each cluster allowed for a linear least squares approach to solve for the DKP. In each nine drifter deployment, 126 different four-drifter combinations exist, so for every 10 minutes of 30-second block averaged drifter observations, 2520 separate calculations of DKP could be computed. As drifters in a cluster move however, it is possible for them to become aligned into a single dimension where DKP calculations are not possible. To account for this, Ohlmann et al. (2016) calculated a cluster aspect ratio, α, for each block averaged drifter cluster as

$$\alpha = \frac{L_{minor}}{L_{major}} \tag{6}$$

where L_{minor} is the minimum distance between drifters in a cluster, and L_{major} is the maximum distance between drifters orthagonal to the L_{minor} direction. Error bar values in DKP calculations approach 1 *f* at $\alpha < 0.2$ so all clusters with ratios less than 0.2 were excluded (Ohlmann et al. 2016). The length scale for each drifter cluster was calculated ($L = (L_{major} + L_{minor})/2$) and DKP values were binned in 20-meter intervals based on their associated length scale.

Calculating the DKP involved adapting an area rate of change method originally used with wind observations (Molinari and Kirwan 1975). In this method, the horizontal divergence is defined as

$$\left(\frac{\partial u}{\partial x} + \frac{\partial v}{\partial y}\right) = \frac{1}{A}\frac{dA}{dt} \tag{7}$$

where the divergence of the parcel (left side) is equal to the horizonal area of the parcel (*A*) times the fractional time rate of change of that horizontal area (*dA/dt*). The horizontal area can be found by using an extension of Bellamy's method to polygons (Davies-Jones 1993). It is defined as

$$A = \frac{\gamma(x, y)}{2} \tag{8}$$

where for a four-sided polygon (γ)

$$\gamma(x, y) = (x_1y_2 - x_2y_1 + x_2y_3 - x_3y_2 + x_3y_4 - x_4y_3 + x_4y_1 - x_1y_4) \tag{9}$$

for any two variables *x* and *y* and when combined with the material derivative of equation (8) yields

$$\frac{1}{A}\frac{dA}{dt} = \frac{\gamma(u, y) + \gamma(x, v)}{\gamma(x, y)} \tag{10}$$

which when equation (10) is inserted to equation (7) gives the divergence of the parcel. To calculate the vorticity, Molinari and Kirwan (1975) showed that a 90 degree clockwise rotation transforms

$$\begin{cases} u \to -v' \\ v \to u' \end{cases} \tag{11}$$

and substituting this into the divergence equation (7) shows that

$$\left(\frac{\partial v}{\partial x} - \frac{\partial u}{\partial y}\right) = \left(\frac{\partial u'}{\partial x} + \frac{\partial v'}{\partial y}\right) \tag{12}$$

where the right-hand side is recognized as

$$\frac{1}{A'}\frac{dA'}{dt} \tag{13}$$

where A' is the area enclosed by the rotated velocity vectors and the time rate of change of this area is the difference between this area and the area from the previous time step. For every 30-second time step, divergence and vorticity were calculated for the associated cluster length scale and binned at 20-meter intervals to sensure a significant number of observations were within each bin.

The Yost IMU dataloggers recorded the rotation rate of the drifter every second, however, after a stationary test of the IMU with no rotation, it was found that they drifted 1 to 2 rotations over an hour even after multiple calibrations, which was an error too large to be used in this experiment due to the few rotations observed in the field.

THIS PAGE INTENTIONALLY LEFT BLANK

III. RESULTS AND DISCUSSION

The DKP calculations were the primary results of the drifter observations and describe the nearshore ocean surface s at scales below 300 meters. A total of 60,704 DKP observations were captured and used to calculate the normalized vorticity in this experiment (Figure 5). All vorticity calculations were normalized by *f*. The distribution of normalized vorticity was very wide with only 7.7 percent of values over 10^2 *f* with a few deployments showing maximum values on the order of 10^5 *f* (not shown on Figure 5). Sixty-five percent of the vorticity observed were between 0 and 20*f*, a range that encompasses nearly all previously observed normalized vorticity including some of the largest measured more recently by Ohlmann et al. (2016) at scales ranging from 300 to 4000 meters. Fifty-six percent of all normalized vorticity observed were positive. This bias towards positive vorticity was most likely from shear caused by the gradient of the mean current flowing south with slower speeds towards land on the east at Point Sal and similarly produced by a westward flowing current on the southern side of Monterey Bay where drifter observations were taken.

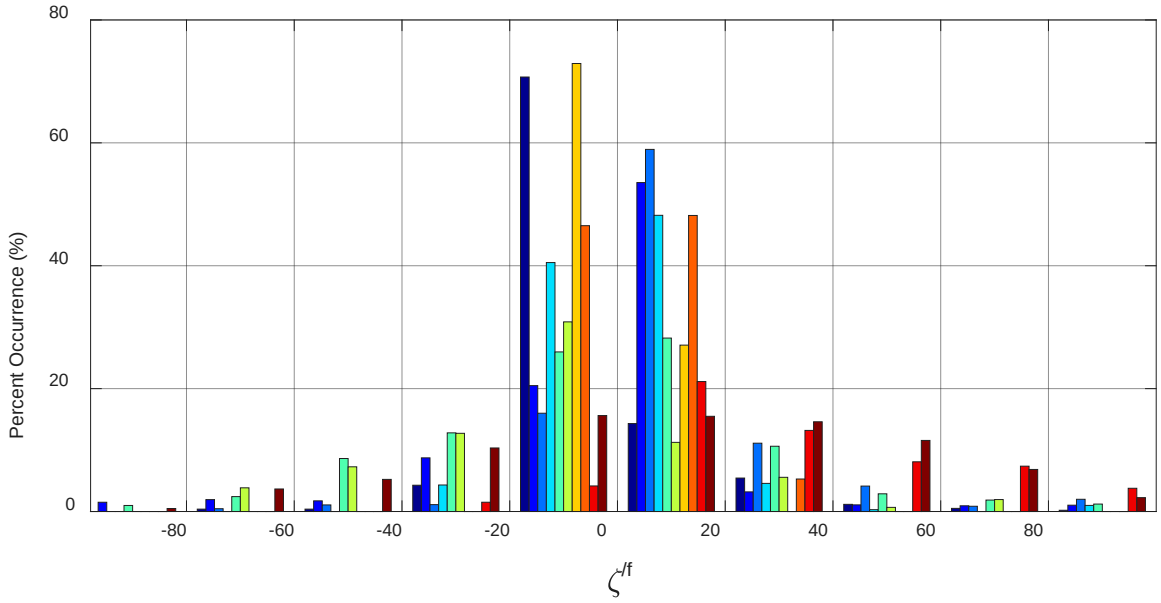

Figure 5. Histogram of normalized vorticity from 10 individual deployments. Values outside of 10^2 *f* excluded (7.7% of values). Each color represents normalized vorticity from separate deployments encompassing all length scales smaller than 300 meters. Bins are 20*f* wide and values are normalized by the total number of observations from that corresponding deployment.

Since DKP calculations were only limited by cluster aspect ratio <0.2 and a length scale of <300 meters, the same set of 60,704 observations were used to calculate normalized divergence in this experiment (Figure 6). All divergence calculations were normalized by *f*. The distribution of normalized divergence was very wide with only 9.5 percent of values over 10^2 *f* with a few deployments showing maximum values on the order of 10^5 *f* (not shown on Figure 6). Forty-two percent of the normalized divergence observed were between 0 and 20*f*, a range that encompasses nearly all previously observed normalized divergence including some of the largest measured more recently by Ohlmann et al. (2016) at scales ranging from 300 to 4000 meters. Thirty-nine percent of all normalized divergence observed were positive. This shows a strong bias towards negative divergence indicating convergence in most of the areas measured.

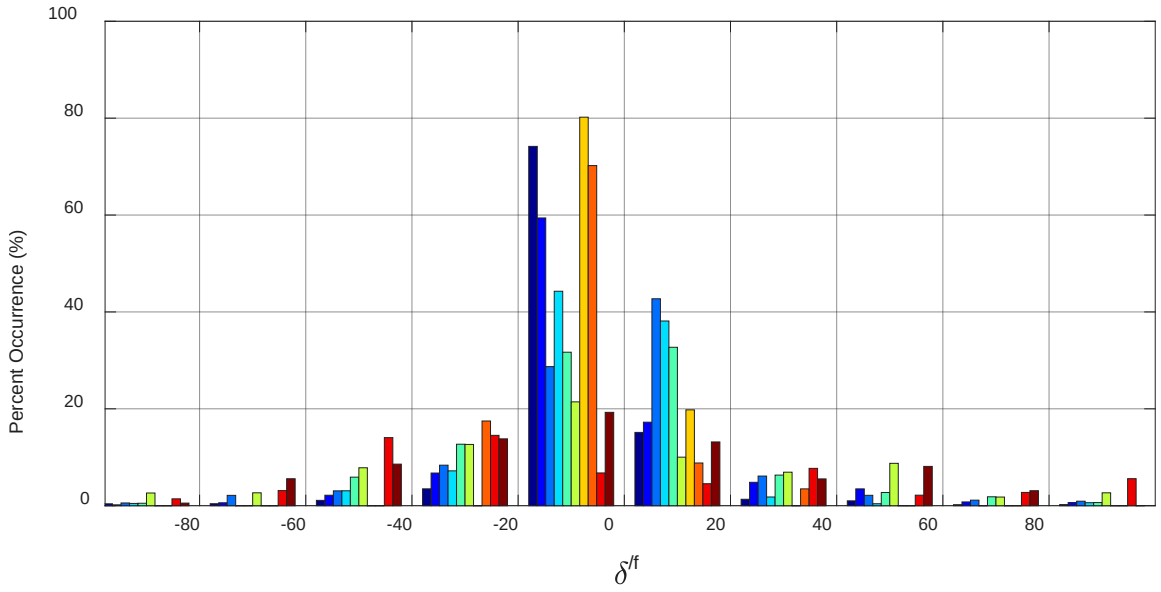

Figure 6. Histogram of normalized divergence from 10 individual deployments. Values outside of 10^2 f excluded (9.5% of values). Each color represents normalized divergence from separate deployments encompassing all length scales smaller than 300 meters. Bins are 20f wide and values are normalized by the total number of observations from that corresponding deployment.

The vorticity calculated with aspect ratio >0.2 were separated by length scale into 20-meter wide bins for all length scales <300 m and the RMS averages $<\zeta^2/f^2>$ were taken for each deployment (Figure 7). 20-meter bins were chosen to have the highest spatial resolution while ensuring at least 30 values were in each bin for each deployment. All values were normalized by f^2. A strong increase in vorticity variance was found for each smaller length scale. This was an extension of the trend in variance found by Ohlmann et al. (2016), shown in black, open circles, and was due to the accumulation of variance from the larger scales (Ohlmann et al. 2016). The increasing trend shows peak RMS values reaching scales approaching 10^5 f^2 at length scales near 10 m.

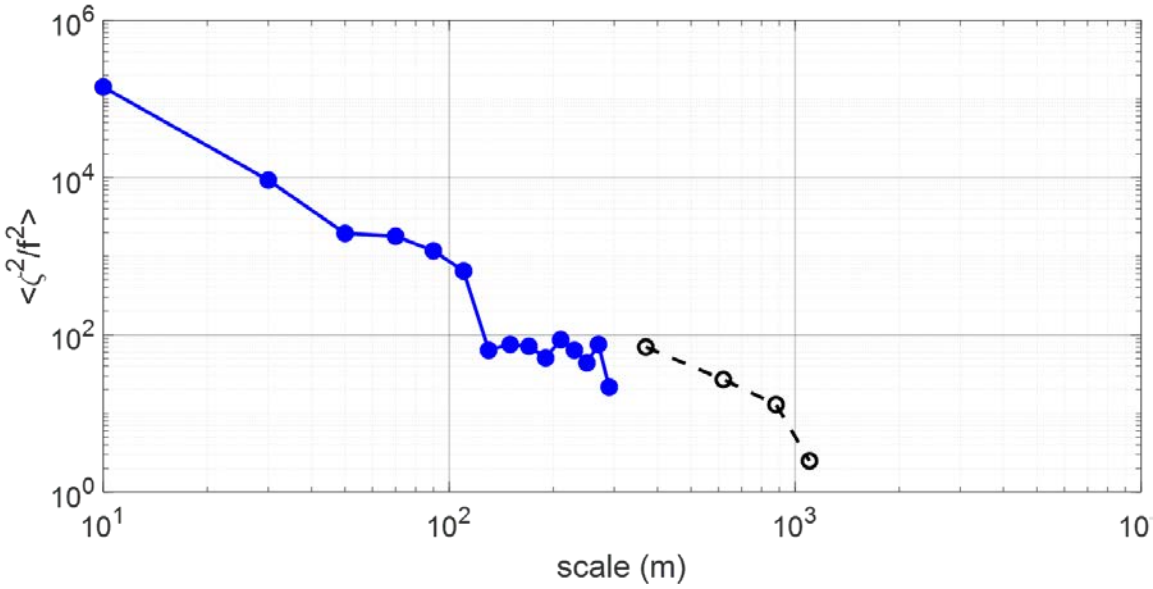

Figure 7. RMS vorticity $<\zeta^2>$ normalized by f^2 as a function of length scale. Solid blue dots are bin averaged vorticity with aspect ratio >0.2 for 20-meter wide bins at length scales less than 300 meters. Black circles are RMS vorticity observed by Ohlmann et al. (2016) with aspect ratio >0.2 averaged in 250-meter wide bins.

The divergence calculations were also RMS averaged $<\delta^2/f^2>$ in the same method as the vorticity for each deployment (Figure 8). The same increase in variance was found matching the variance trends from vorticity and divergence by this study and by Ohlmann et al. (2016). This trend had more noise though due to the inability to capture completely homogeneous samples with Lagrangian drifters. This trend was also due to the accumulation of variance from each larger length scale reaching peak RMS values on the order of $10^5 f^2$ on average for length scales near 10 m.

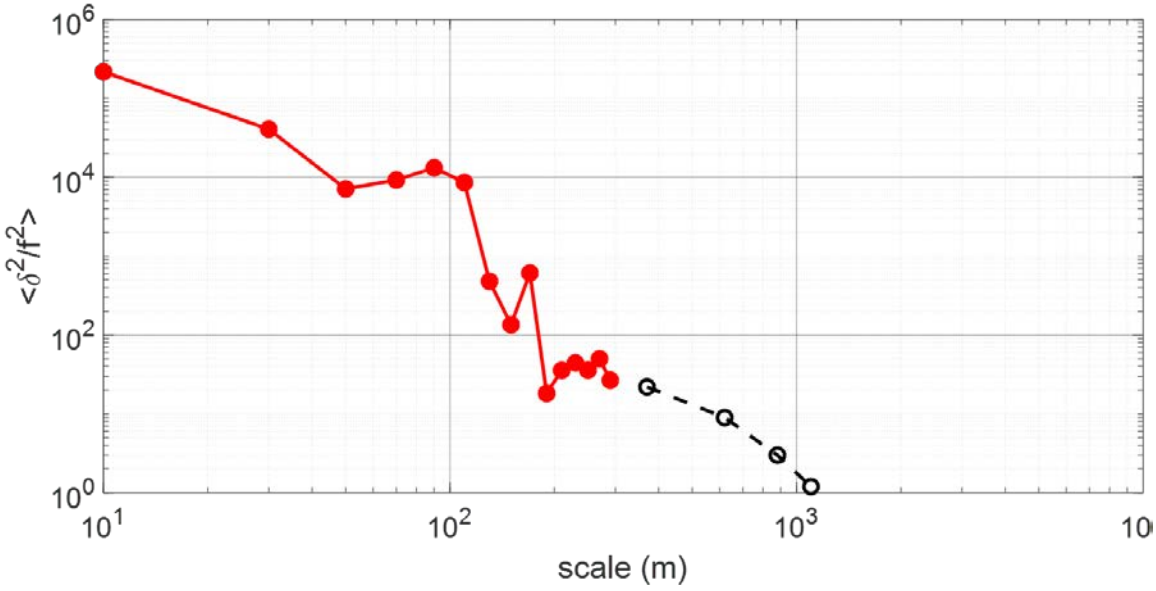

Figure 8. RMS divergence $<\delta^2>$ normalized by f^2 as a function of length scale. Solid blue dots are bin averaged divergence with aspect ratio >0.2 for 20-meter wide bins at length scales less than 300 meters. Black circles are RMS divergence observed by Carter et al. (2016) with aspect ratio >0.2 averaged in 250-meter wide bins.

These DKP calculations were from drifter clusters deployed in visually energetic areas such as areas of visually turbulent flows, noticeable shear, eddies, and frontal regions resulting in large values of vorticity and divergence. These large values are caused by flows interacting with coastal bathymetry, shear induced by coastal gradients in currents, and influences from larger scale features.

THIS PAGE INTENTIONALLY LEFT BLANK

IV. CONCLUSION

This study investigated the DKP of submesoscale flows in the nearshore at scales smaller than 300 m. It looked at the vorticity and divergence of these flows using purpose-built vorticity drifters capable of observing the individual rotation of the 1-m diameter parcel of water it was submerged in and the properties of larger scale flows using drifter clusters with average position error on the order of 11 cm and average moving speed error on the order of 0.7 cm/s. Using this approach, large ageostrophic flows caused by submesoscale turbulence were observed in the nearshore. The decreases in position error and speed error allowed for DKP observations at scales smaller than previously observed. At these scales RMS vorticity and divergence values continued their previously observed upward trend and reached a peak value on the order of $10^5 f^2$ at the averaged length scale of 10 m, the largest value observed to date. The flow s observed by this study provide further insight into the submesoscale turbulence that occurs and the influence it has on mixing at these small scales.

While the vorticity drifter constructed for this experiment was capable of rotating with a 1-m parcel of water, the Yost IMU was incapable of recording the rotation rate due to the drift of the IMU. The IMU was found to have 1 to 2 rotations of drift over an hour during a stationary test that was on the same order of the rotation rate observed in the field. Future experiments would benefit from using a more precise IMU such as the Lowell Instruments MAT-1 Data Logger (https://lowellinstruments.com/products/mat-1-data-logger/), which was found after the experiment to have less than one degree of drift over a one-hour stationary test. With this IMU, vorticity could be recorded all the way down to one meter. This would allow for the capture and measurement of submesoscale vorticity in nearshore energetic zones as done in this experiment.

THIS PAGE INTENTIONALLY LEFT BLANK

LIST OF REFERENCES

Capet, X., J. C. McWilliams, M. J. Molemaker, and A. Shchepetkin, 2008a: The transition from mesoscale to submesoscale in the California Current System. Part I: Flow structure, eddy flux and observational tests. *J. Phys. Oceanogr.*, **38**, 29–43, https://doi.org/10.1017/jfm.2012.90.

Capet, X., J. C. McWilliams, M. J. Molemaker, and A. Shchepetkin, 2008b: The transition from mesoscale to submesoscale in the California Current System. Part II: Frontal processes. *J. Phys. Oceanogr.*, **38**, 44–64, https://doi.org/10.1175/2007JPO3672.1.

d'Ovidio, F., J. Isern-Fontanet, C. López, E. Hernández-García-Ladona, 2009: Comparison between Eulerian diagnostics and finiti-size Lyapunov exponents computed from altimetry in the Algerian basin. *Deep Sea Res.*, **56**, 15–31, https://doi.org/10.1016/j.dsr.2008.07.014.

Davies-Jones, R., 1993: Useful, Formulas for Computing Divergence, Vorticity, and Their Errors from Three or More Stations. *Mon. Wea. Rev.*, **121**, 713–725, https://doi.org/10.1175/1520-0493(1993)121<0713:UFFCDV>2.0.CO;2

LaCasce, J. H., and J. C. Ohlmann, 2003: Relative dispersion at the surface of the Gulf of Mexico. *J. Mar. Res.*, **61**, 285–312, https://doi.org/10.1357/002224003322201205.

LeHahan, Y., F. d'Ovidio, M. Lévy, and E. Heifetz, 2007: Stirring of the northeast Atlantic spring bloom: A Lagrangian analysis based on multisatellite data. *J. Geophys. Res.*, **112**, C08005, https://doi.org/10.1029/2006JC003927.1.

MacMahan, J., J. Brown, and E. Thornton, 2009: Low-cost handheld global positioning system for measuring surf-zone currents. *J. Coastal Res.*, **25**, 3, 744–754.

Mahadevan, A., and A. Tandon, 2006: An analysis of mechanisms for submesoscale vertical motion at ocean fronts. *Ocean Model.*, **14**, 241–256, https://doi.org/10.1029/2008JC005203.

McWilliams, J. C., 2016: Submesoscale currents in the ocean. *Proc. R. Soc. A*, **472**, 20160037, https://doi.org/10.1098/rspa.2016.0117.

McWilliams, J. C., M. J. Molemaker, and I. Yavneh, 2001: From stirring to mixing of momentum: Cascades from balanced flows to dissipation in the oceanic interior. *Aha Huliko'a Proceddings*. 59–66.

Molemaker, M. J., J. C. McWilliams, and X. Capet, 2010: Balanaced and unbalanced routes to dissipation in an equilibrated Eady flow. *J. Fluid Mech.*, **654**, 35–63, https://doi.org/10.1017/S0022112009993272.

Molinari, R. and A. D. Kirwan, 1975: Calculations of differential properties from Lagrangian observations in the Western Caribbean Sea. *J. Phys. Oceanogr.*, **5**, 483–491, https://doi.org/10.1175/1520-0485(1975)005<0483:CODKPF>2.0.CO;2.

Muller, P., J. McWilliams, and J. Molemaker, 2005: Routes to dissipation in the ocean: The 2D/3D turbulence conundrum, in Marine Turbulence: Theories, Observations and Models, edited by H. Baumert, J. Simpson, and J. Sundermann, pp. 397–405, Cambridge univ. Press, Cambridge.

Ohlmann, J. C., M. J. Molemaker, B. Baschek, B. Holt, G. Marmorino, and G. Smith, 2017: Drifter observations of submesoscale flow s in the coastal ocean. *Geophys. Res. Lett.*, **44**, 330–337, https://doi.org/10.1002/2016GL071537.

Rudnick, D. L., 1996: Intensive surveys of the Azores Front: 2. Inferring the geostrophic and vertical velocity fields. *J. Geophys. Res.*, **101**, 16291-16303, https://doi.org/10.1029/96JC01144.

Saeki, M. and M. Hori, 2006: Development of an accurate positioning system using low-cost L1 GPS receivers. *Computer-Aided Civil & Infrastructure Engineering*, **21**, 258–267.

Schmidt, W., B. Woodward, K. Millikan, R. Guza, B. Raubenheimer, and S. Elgar, 2003: A GPS-tracked surf zone drifter. *Journal of Atmospheric and Oceanic Technology*, **20**, 1069–1075.

Shearman, R. K., J. M. Barth, and P. M. Kosro, 1999: Diagnosis of three-dimensional circulation associated with mesoscale motion in the California current. *J. Phys. Oceanogr.*, **29**, 651–670.

Swenson, M. S., and P. P. Niiler, 1996: Statistical analysis of the surface circulation of the California Current. *J. Geophys. Res.*, **101**, 22631-22645, https://doi.org/10.1029/96JC02008.

INITIAL DISTRIBUTION LIST

1. Defense Technical Information Center
   Ft. Belvoir, Virginia

2. Dudley Knox Library
   Naval Postgraduate School
   Monterey, California